Geophysical Journal International

Geophys. J. Int. (2018) **214,** 1252–1266
Advance Access publication 2018 May 16
GJI Geodynamics and tectonics

doi: 10.1093/gji/ggy189

The influence of lateral Earth structure on glacial isostatic adjustment in Greenland

Glenn A. Milne,[1] Konstantin Latychev,[2] Andrew Schaeffer,[1] John W. Crowley,[1,3] Benoit S. Lecavalier[4] and Alexandre Audette[1]

[1]*Department of Earth and Environmental Sciences, University of Ottawa, Ottawa, ON* K1N 6N5, *Canada. E-mail: gamilne@uottawa.ca*
[2]*Department of Earth and Planetary Sciences, Harvard University, Cambridge, MA* 02138, *USA*
[3]*Canadian Geodetic Survey, Natural Resources Canada, Ottawa, ON* K1A 0Y7, *Canada*
[4]*Department of Physics and Physical Oceanography, Memorial University of Newfoundland, St. John's, NL* A1C 5S7, *Canada*

Accepted 2018 May 15. Received 2018 May 10; in original form 2017 July 16

SUMMARY

We present the first results that focus on the influence of lateral Earth structure on Greenland glacial isostatic adjustment (GIA) using a model that can explicitly incorporate 3-D Earth structure. In total, eight realizations of lateral viscosity structure were developed using four global seismic velocity models and two global lithosphere (elastic) thickness models. Our results show that lateral viscosity structure has a significant influence on model output of both deglacial relative sea level (RSL) changes and present-day rates of vertical land motion. For example, lateral structure changes the RSL predictions in the Holocene by several tens of metres in many locations relative to the 1-D case. Modelled rates of vertical land motion are also significantly affected, with differences from the 1-D case commonly at the mm yr^{-1} level and exceeding 2 mm yr^{-1} in some locations. The addition of lateral structure considered here is unable to account for previously identified data model RSL misfits in northern and southern Greenland, suggesting limitations in the adopted ice model and/or the existence of processes not included in our model. Our results show large data model discrepancies in uplift rates when applying a 1-D viscosity model tuned to fit the RSL data; these discrepancies cannot be reconciled by adding the realizations of lateral structure considered here. In many locations, the spread in model output for the eight different 3-D earth models is of similar amplitude or larger than the influence of lateral structure (as defined by the average of all eight model runs). This reflects the differences between the four seismic and two lithosphere models used and implies a large uncertainty in defining the GIA signal given that other aspects that contribute to this uncertainty (e.g. scaling from seismic velocity to viscosity) were not considered in this study. In order to reduce this large model uncertainty, an important next step is to develop more accurate constraints on Earth structure beneath Greenland based on regional geophysical data sets.

Key words: Structure of the Earth; Loading of the Earth; Sea level change; Numerical modelling; Rheology: mantle.

1 INTRODUCTION

The response of the solid Earth and gravity field to mass changes in ice sheets and glaciers is recorded in various data types, including proxy observations of relative sea level (RSL) change reconstructed from geological records and present-day changes in land motion and gravity. Modelling these data sets has provided information on both the rheological properties of the mantle and the spatiotemporal history of ice extent (e.g. Peltier & Andrews 1976; Wu & Peltier 1983; Tushingham & Peltier 1991; Mitrovica 1996; Lambeck *et al.* 1998; Milne *et al.* 2001; Tamisiea *et al.* 2007). Recently, research within this discipline, known as glacial isostatic adjustment (GIA), has focused on the regions occupied by the contemporary ice sheets given the expected continuation of climate warming and the potential contribution of the Greenland and Antarctic ice sheets to future sea level rise.

Studies of GIA are relevant to the aim of making improved projections of the contemporary ice sheets in several respects. For example, GIA-related data sets are sensitive to the evolution of the ice sheets during the most recent glacial to interglacial transition and so provide important observational constraints for testing models

of ice sheet evolution on century to millennial timescales and producing model reconstructions of changes in ice extent since the last glacial maximum (e.g. Tarasov & Peltier 2002; Fleming & Lambeck 2004; Ivins & James 2005; Simpson *et al.* 2009; Whitehouse *et al.* 2012; Lecavalier *et al.* 2014). In turn, these model reconstructions are used to remove the GIA contribution from geodetic observations in order to estimate ice mass changes in recent decades (e.g. Shepherd *et al.* 2012), which provide initial conditions for model runs of future ice sheet changes. As GIA-related data sets and models improve, so does the accuracy to which these procedures can be performed. Here we report on an advance in modelling GIA in Greenland and discuss the implications this has for applying these procedures in this region.

Recent advances in our understanding of Greenland GIA have been driven, primarily, by improvements in data quality and quantity. Concentrated field efforts have led to a dramatic increase in the spatial and temporal coverage of ice extent (e.g. Funder *et al.* 2011; Sinclair *et al.* 2016) and relative sea level (Long *et al.* 2011) reconstructions. Installation of a circum-Greenland network of continuously operating global positioning system (GPS) receivers (Bevis *et al.* 2012) is also now yielding information that can be applied in regional scale GIA modelling (Khan *et al.* 2016). These improvements in data control have been incorporated into modelling studies that focused on producing deglacial model reconstructions of the Greenland ice sheet (Tarasov & Peltier 2002; Fleming & Lambeck 2004; Simpson *et al.* 2009; Lecavalier *et al.* 2014; Khan *et al.* 2016). In some of these studies (Simpson *et al.* 2009; Lecavalier *et al.* 2014; Khan *et al.* 2016), it was found that model fits could be improved by invoking lateral changes in Earth viscosity structure. However, all of these studies were based on spherically symmetric earth models and so lateral viscosity variations were not rigorously treated.

A number of studies have applied 3-D earth models in regional, near-field GIA analyses, including North America (e.g. Wu 2006; Paulson *et al.* 2007), Fennoscandia (e.g. Steffen *et al.* 2006; Whitehouse *et al.* 2006; van der Wal *et al.* 2013) and Antarctica (e.g. Kaufmann *et al.* 2005; van der Wal *et al.* 2015). In all of these studies, lateral viscosity structure is shown to have a significant impact on predictions of GIA-related observables, implying that inferences of model parameters relating to the ice history or viscosity structure based on 1-D (spherically symmetric) models could be biased and thus impact the GIA model applications outlined above.

To our knowledge, only Xu *et al.* (2016) have applied a 3-D earth model to determine the GIA signal in Greenland. The focus of Xu *et al*. was to estimate present-day ice sheet mass balance via two different methods (satellite gravity and the so-called "input–output" method) and compare the results. As indicated in their Table A3, two GIA model runs were performed that included laterally variable Earth structure. The results provided in their Table A3 give an indication of the impact of lateral structure on gravity-based estimates of the regional ice sheet mass balance changes in Greenland. However, since the focus of Xu *et al.* (2016) was not on the impact of lateral structure on Greenland GIA, few details are provided on this aspect of the analysis (e.g. how lateral structure was defined, its uncertainty and impact on other GIA-related observables such as RSL and vertical land motion).

This is the first study to consider, in depth, the influence of lateral viscosity structure on GIA in Greenland. Given the recent advances in observational constraints and the growing evidence for the importance of lateral structure in this region (Simpson *et al.* 2009; Khan *et al.* 2016), the motivation for such a study is evident. Our primary aim is to quantify the effect of large-scale lateral viscosity structure on model output of GIA and discuss the results with regard to some of the GIA model applications described above. Specifically, can the addition of lateral structure explain some large data model residuals reported for RSL (e.g. Lecavalier *et al.* 2014; Woodroffe *et al.* 2014) and GPS (Khan *et al.* 2016) observations and how might current ice model reconstructions be biased by not considering lateral Earth structure.

One difficulty in quantifying the effect of lateral Earth structure on model output is the uncertainty in defining this structure. Thermal and compositional variations are the primary drivers of large-scale lateral variability in mantle viscosity structure (Karato 2008; Stixrude and Jeanloz 2015). Some evidence suggests that thermal effects are dominant in the upper mantle (e.g. Cammarano *et al.* 2011). Given the lack of quantitative information on which of these two factors dominate and where in the mantle, some previous studies have used GIA observables in an effort to determine the relative importance of thermal and compositional effects (Wang *et al.* 2008; Wu *et al.* 2013). While the results of these studies demonstrate clear potential for this approach, robust estimates are not yet available due to the difficulty in adequately exploring the model parameter space as well as limitations in the data. The results of Wu *et al.* (2013), which consider observations from Fennoscandia, suggest that temperature is the dominant control in this region, ranging from 65 per cent dominant in the upper mantle and increasing with depth in the lower mantle; although the uncertainty in this inference also increases significantly with depth. Given the difficulty in exploring the model parameter space due to the high computational cost of 3-D earth models, we follow a more simplistic approach here and assume that lateral variations in viscosity structure are driven by temperature only. As described in Section 2.2, we estimate temperature variations based on realizations of seismic velocity structure assuming that compositional changes have a negligible effect on the velocity variations. Our motivation for choosing this approach is that we can focus on another aspect of uncertainty in defining the lateral variability in viscosity not yet introduced: that of the input seismic velocity model. Indeed, a secondary aim of this analysis is to quantify the influence of this uncertainty source by considering four recently published seismic velocity models. We also consider two models of lithospheric elastic thickness variations to arrive at a total of eight different realizations of lateral viscosity structure. Although this is a relatively small ensemble of models compared to analyses based on 1-D earth models (e.g. Lecavalier *et al.* 2014), considering a larger number is difficult given the high computational expense of the applied numerical model (Latychev *et al.* 2005). Of course, the above assumptions and the limited size of the model ensemble limit the generality of the conclusions that can be drawn from the results presented in Section 3. That said, we believe our results represent an important first step towards quantifying the uncertainty of 3-D earth models applied to study GIA in Greenland.

2 METHODS

2.1 GIA model

The results presented below were generated using a numerical finite-volume formulation of the surface loading process (Latychev *et al.* 2005). This formulation solves the underlying equations for the case of a Maxwell viscoelastic rheology within a spherical tetrahedral grid in which the grid resolution is variable and greatest near the model earth surface. At the surface, the lateral resolution is ∼15 km, compared to ∼60 km at the core–mantle boundary. The depth resolution varies from ∼12 km immediately beneath the

surface to ∼50 km immediately above the core–mantle boundary. The model computes a number of observables, including RSL and rates of present-day vertical land motion and geoid change, for a specified surface (ice) loading history and Earth density and viscoelastic structure. The associated ocean loading is computed by solving the sea level theory and algorithm described in Kendall *et al.* (2005) and so time-varying coastlines are incorporated. We note that the version of the model applied here extends the algorithm of Kendall *et al.* (2005) to include the influence of earth rotation on model output (Milne & Mitrovica 1998; Mitrovica *et al.* 2005). Displacements at the model earth surface are computed relative to the centre of mass of the Earth and surface load (i.e. the 'CM' reference frame; Blewitt 2003), which can lead to long-wavelength, sub-mm yr^{-1} residuals when comparing model output to GPS-inferred vertical motion for high-latitude regions such as Greenland (Section 3.2; Argus 2012). The ice history is a combination of models from previous studies. The Greenland component is the so-called Huy3 model reconstruction presented in Lecavalier *et al.* (2014), which was tuned to fit a regional database of RSL and ice extent constraints. The model was first tuned to fit ice extent constraints and then 1-D earth viscosity model parameters (see the next paragraph) were identified that optimized model fits to the RSL data. For the North American ice complex (comprising the Cordilleran, Innuitian and Laurentide ice sheets), we adopt a model reconstruction (termed nn9894) from Tarasov *et al.* (2012) that provided some of the best fits to a regional database of RSL, ice extent and present-day vertical land motion. For the remaining ice sheets, we use the commonly applied ICE-5G model reconstruction described in Peltier (2004). The three ice model reconstructions were produced using different methodologies; for example, the Huy3 and nn9894 histories are generated from output of numerical thermomechanical ice models with user-specified forcings and boundary conditions, whereas the ICE-5G model is not based on output from a glaciological model (except for the Greenland component, which is not used here). Also, the process through which best-fitting model parameters were identified range in complexity and rigour, with that applied in Tarasov *et al.* (2012) being the more robust of the three studies. Finally, we note that the nn9894 and ICE-5G models were determined assuming a given 1-D earth viscosity model (VM5a for nn9894 and VM2 for ICE-5G). For further information on the ice loading histories applied here, the reader is referred to the original publications.

The density and elastic structure of the model earth are defined to be depth-dependent only and are based on the preliminary reference earth model (Dziewonski & Anderson 1981). In total, nine earth viscosity models were considered to assess the sensitivity of model output to this key input. To serve as a reference case, we performed one run with no lateral variations in which the depth-dependent structure is given by a lithospheric (elastic) thickness of 120 km, a uniform upper-mantle (base of lithosphere to 670 km depth) viscosity of 5×10^{20} Pa s and a uniform lower-mantle (670 km to the base of the mantle) viscosity of 2×10^{21} Pa s. This 1-D viscosity model optimized the fit to a regional data set of RSL change when using the Huy3 ice loading history (Lecavalier *et al.* 2014). This viscosity model is also very similar to the so-called VM2 model (Peltier 2004) that was used in generating the nn9894 ice history (Tarasov *et al.* 2012) and ICE-5G. Lateral viscosity variations were added to the reference 1-D structure by using four global seismic velocity models to estimate lateral temperature and therefore viscosity variations. Lateral variations in lithospheric (elastic) thickness were also applied via two published estimates of this structure (Zhong *et al.* 2003; Conrad & Lithgow-Bertelloni 2006). Further information on these realizations of lateral structure is provided in the following section.

By considering four different seismic tomography models and two different estimates of lithospheric (elastic) thickness, a total of eight realizations of lateral viscosity structure were input to the model. Output from this set of eight inputs is compared to that generated for the reference (1-D) case in Section 3. To consider the sensitivity of model output to structure at different depth ranges, we performed three additional runs for the GIA model with lateral structure based on the S40RTS seismic velocity model (introduced below). Thus, the results in Section 3 represent a total of 12 model runs (including the reference 1-D case). Each model run takes ∼5 days on 114 compute cores and so the results presented below represent a total of computation time of just under 6900 core days.

2.2 Estimates of lateral viscosity structure

The two global lithosphere thickness models we apply are based on different methods and observations over continental regions. The model presented by Zhong *et al.* (2003) is based on the results of loading studies and heat flux observations, whereas that presented in Conrad & Lithgow-Bertelloni (2006) is based on the depth to a defined (minimum) seismic velocity perturbation (ostensibly a thickness estimate of the thermal lithosphere). Over ocean areas, the thickness estimates are related to either lithospheric age (Conrad & Lithgow-Bertelloni 2006) or the depth to a specified geotherm calculated using the half-space cooling model (Zhong *et al.* 2003). Given that the age and thermal structure of the oceanic lithosphere are related, the estimates in oceanic areas show similar variations in the two models. For further details, the reader is referred to the original articles. In the majority of GIA modelling studies, the lithosphere is defined by assigning very high viscosity values such that it acts elastically over GIA timescales. Thus, the methods used to define the two models used here provide only an approximate estimate of this quantity.

The two lithosphere thickness models were scaled such that the global mean is the same as that in our 1-D reference model (120 km). Fig. 1 shows the thickness distribution of both models after this scaling was applied. Both models show the thinnest lithosphere in the vicinity of the mid-Atlantic ridge with a progressive thickening towards Greenland. The greatest differences between the two models are, as expected, over continental areas, with the scaled Conrad and Lithgow-Bertelloni model exhibiting considerably thicker values over all of Greenland except for the southeast. The greatest differences are evident in northeast Greenland where they exceed 100 km. These differences are large and reflect the methods applied as well as the difficulty in estimating the mechanical (elastic) thickness of the lithosphere, particularly in ice-covered continental areas. Of these two models, that by Zhong *et al.* (2003) is most consistent with a recent inference of thermal elastic thickness in central Greenland (Petrunin *et al.* 2013), which indicates that the lithosphere is relatively thin for an early Proterozoic terrain and increases in thickness from east to west by ∼30 km over central Greenland (based on the depth to the 1300°C isotherm).

As stated above, four global seismic velocity models were used to estimate lateral viscosity variations beneath the model lithosphere. These models are: S40RTS (Ritsema *et al.* 2011), Savani (Auer *et al.* 2014), SEMUCB-WM1 (French & Romanowicz 2014) and SL2013sv (Schaeffer & Lebedev 2013). Each model defines lateral deviations in shear wave velocity relative to a reference 1-D velocity profile. All models provide lateral velocity variations throughout

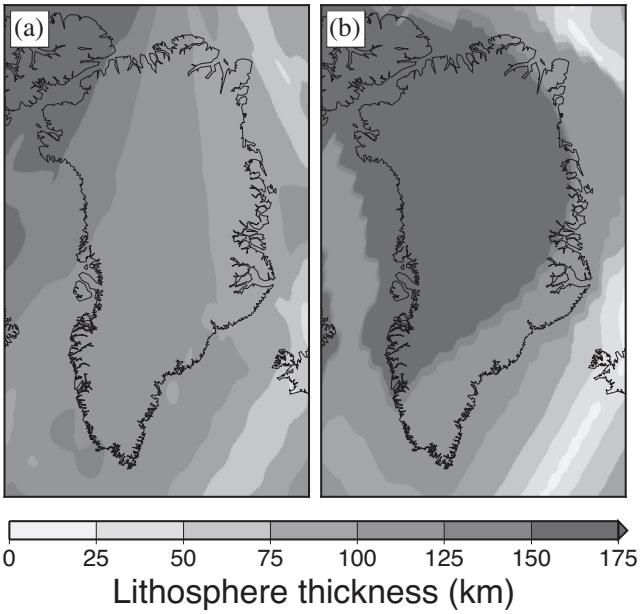

Figure 1. Variations in elastic thickness across the study region based on two published global models: (a) Zhong *et al.* (2003) and (b) Conrad & Lithgow-Bertelloni (2006). Both models were scaled to produce a global average thickness equal to that of the reference 1-D model (120 km).

the whole mantle with the exception of SL2013sv, which extends to only ∼1000 km depth; the shear velocity below this depth follows that of the 1-D model AK135 (Kennett *et al.* 1995). These particular models were chosen because they are relatively recent and represent development by different research groups. Also, while there is some overlap in the data sets used in their construction, there are also clear differences in both the data sets employed and the modelling (forward and inverse) methods used.

S40RTS is an isotropic shear velocity model of the mantle constrained by three data sets: minor and major arc Rayleigh wave dispersion, teleseismic body-wave traveltimes and spheroidal mode splitting functions; the ray-theoretical great circle path propagation is assumed and inversion is carried out using a damped least-squares approach. SEMUCB-WM1 is a Voigt-average shear speed and radial anisotropy model constrained by long-period waveforms (multimode Rayleigh and Love waves and long-period body waves) and group-velocity dispersion maps; a hybrid waveform inversion approach combines a spectral finite element method (SEM) for forward modelling with non-linear asymptotic coupling for the inverse step to improve computational efficiency. Savani is a radially anisotropic shear wave velocity model of the whole mantle constructed with a variably parametrized grid adapted to reflect the relative data coverage in each grid cell. The data includes phase delays measured for the fundamental and first five overtones of Rayleigh and Love waves, as well as body-wave traveltime delays for a variety of *S*-wave phases. Finally, SL2013sv is a vertically polarized shear velocity model of the upper mantle, transition zone and uppermost lower-mantle, constrained by a very large data set of seismograms successfully fit using an automated multimode waveform inversion approach. Approximate sensitivity volumes enable improved accuracy compared to pure ray theory; in addition, a 3-D crustal model is solved for during the inversion, minimizing the propagation of artefacts into the mantle due to corrections based on assumed crustal structure. Inversion is carried out via an iterative least squares approach. Although cases can be made for the veracity of one model over another in the vicinity of Greenland, for the purpose of this study, we consider each to represent an equally probable realization of Earth velocity structure.

We follow the method described in Latychev *et al.* (2005) to determine viscosity structure from seismic velocity variations. This method applies the assumption that compositional changes have a small influence on the lateral velocity perturbations and so can be ignored. In doing so, three equations can be applied to convert the velocity perturbations to viscosity changes. The first step involves converting the velocity variations into density structure via

$$\delta \ln \rho\,(r,\theta,\varphi) = \left[\frac{\delta \ln \rho\,(r)}{\delta \ln v_s\,(r)}\right] \delta \ln v_s\,(r,\theta,\varphi)\,, \tag{1}$$

where v_s and ρ are perturbations in shear wave speed and density as a function of radius (r), colatitude (θ) and east longitude (φ). A depth-dependent scaling factor shown by the term in square brackets is used to convert velocity structure to density structure. We adopt the profile presented in Forte & Woodward (1997) to define this scaling.

The second step involves converting density structure to variations in temperature (T) via the material property known as the volume coefficient of thermal expansion (α), as given by the relationship

$$\delta T\,(r,\theta,\varphi) = -\frac{1}{\propto (r)}\,\delta \ln \rho\,(r,\theta,\varphi)\,. \tag{2}$$

We adopt the depth dependence of the parameter α as derived by Chopelas & Boehler (1992). The third and final step involves calculating the viscosity (ν) variations by adopting the relationship

$$\nu\,(r,\theta,\varphi) = \nu_0\,(r)\,\mathrm{e}^{-\epsilon \delta T(r,\theta,\varphi)}, \tag{3}$$

where $\nu_0(r)$ is the 1-D reference viscosity profile and ϵ is a free parameter that defines the strength of the temperature changes on viscosity. In all of our calculations we define ϵ to be a constant value of 0.04 $^{\circ}\mathrm{C}^{-1}$, which leads to lateral viscosity variations of around five orders of magnitude in our study region (Fig. 2 and Figs S1–S4, Supporting Information). We believe this relatively large range is reasonable given that the region includes old and stable continental cratons as well as divergent plate boundaries and a hotspot (Iceland). The above procedure to convert seismic velocity to viscosity accounts for both anharmonic and anelastic effects as both are included in the adopted profile of perturbations in density relative to perturbations in shear wave velocity (bracketed term on the right-hand side of eq. 1; Karato 1993). It is important to note that the parameters adopted in the above scaling relations contain significant uncertainty (e.g. Ivins & Sammis 1995).

The lateral structure is defined first on some pre-determined set of radii that depend on the adopted seismic model. Next, these fields are interpolated to other radial layers (at higher resolution than that provided in the seismic models) via radial splines. Note that lateral variations are not applied within the lower 100 km or so of the mantle given the expected large contribution of chemical heterogeneity in this region to both seismic velocity and viscosity structure (which are assumed negligible in this study). Thus, the viscosity will be laterally uniform and equal to the reference 1-D model in this part of the lower mantle. This is not a concern given that the GIA observables considered here are insensitive to structure in the deep lower mantle.

We chose three depths, 200, 600 and 1000 km, to illustrate the typical amplitude and variation of lateral structure inferred from the shear wave velocity models. The viscosity variations for these

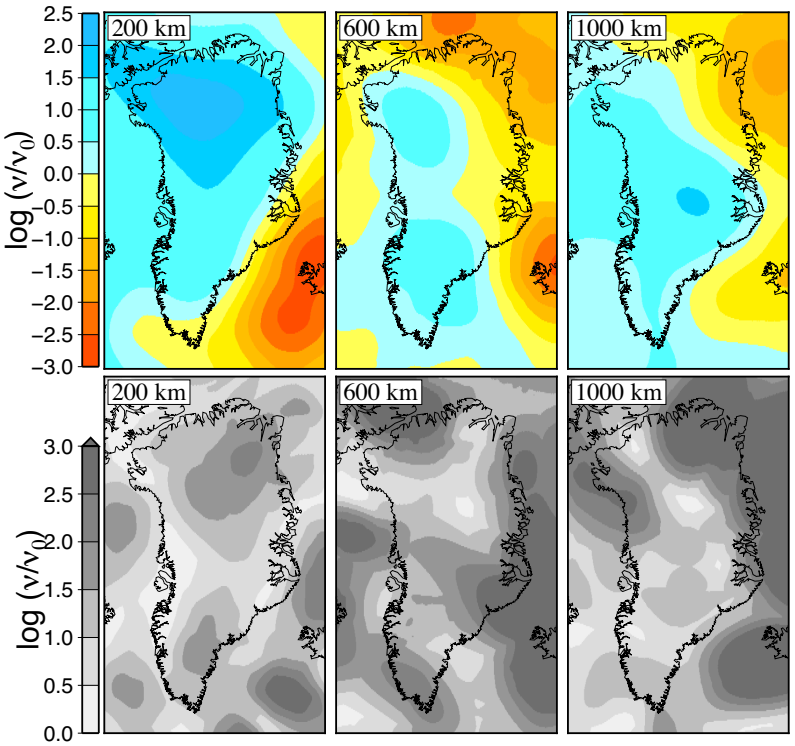

Figure 2. Top frames show the mean viscosity computed from all four seismic models considered, relative to the value in the reference 1-D model (i.e. 5×10^{20} Pa s in the upper mantle and 2×10^{21} Pa s in the lower mantle), at three different depths. The bottom frames indicate the total range in viscosity values.

depths are shown for each seismic model in the Supporting Information (Figs S1–S4). Inspection of these figures shows that, while there are similarities between the viscosity variations for each model, there are also considerable differences. (Note that the SL2013sv model shows less viscosity structure compared to the other models at 1000 km depth given the relatively limited depth resolution of this model, which drops off below depths of about 800 km.) For example, all models show low viscosities in the vicinity of the Iceland hotspot but there are differences in the location of and the lateral/vertical extent of this feature. Also, some models appear to resolve structure better than others at certain depths: for example, the SEMUCB-WM1 and SL2013sv models appear to better resolve the fast velocity (high viscosity) anomaly beneath Greenland at 200 km depth. These differences reflect the data and methods used in constructing the four seismic models described above. Fig.2 summarizes the results in Figs S1–S4 of the Supporting Information by showing the mean (top frames) and the range (i.e. greatest difference; bottom frames) in viscosity when considering all four models. The most robust features are evident in the mean, including the lower viscosities (slower wave speeds) to the east of Greenland and higher viscosities beneath Greenland, with lateral variations reaching about five orders of magnitude. As evident in the differences shown between Figs S1 and S4 of the Supporting Information, the range in viscosity values between the four models is large; reaching several orders of magnitude in many areas (see lower frames in Fig. 2). The largest differences between models are found east of Greenland for the 600 and 1000 km depth slices, reflecting the large lateral velocity gradients in this region.

As outlined in Section 1, there are a number of sources of uncertainty in determining estimates of lateral viscosity variations in the mantle. A primary one is the uncertainty in the velocity models as the results in Fig.2 (lower frames) indicate. By using four velocity models that are based on different data sets and modelling approaches, we can quantify, albeit crudely, the influence of this source of uncertainty. A four-model sample set is limited but using a larger number is difficult given the relatively small number of global seismic models that are produced by independent research groups and the high computational expense of the GIA model applied here. The other primary sources of uncertainty are: (1) the assumption that velocity heterogeneity is the result of temperature variations only and (2) viscosity variations are driven by temperature only. The accuracy of the first assumption will vary within the mantle and is poor where there are significant lateral variations in properties other than temperature that affect the bulk density or shear elastic properties of rock (Priestley & McKenzie 2013). Regarding the second, it will be less accurate in regions where other factors vary that are known to influence the ductile behaviour of rock, such as composition, structure (e.g. grain size) or volatile content (Karato 2008).

3 RESULTS AND DISCUSSION

3.1 Relative sea level

The contribution of GIA to RSL change around Greenland is illustrated in Fig. 3. Model output based on the 1-D reference earth model (top-left frame and black lines in other frames) as well as reconstructed RSL changes are shown for seven sites around Greenland. These (1-D) model results reflect those in Lecavalier *et al.* (2014) since they are based on the same Greenland ice model reconstruction (Huy3) and earth viscosity model. The non-Greenland component of the ice model is also the same except that here we used a different model reconstruction for the North American ice sheets

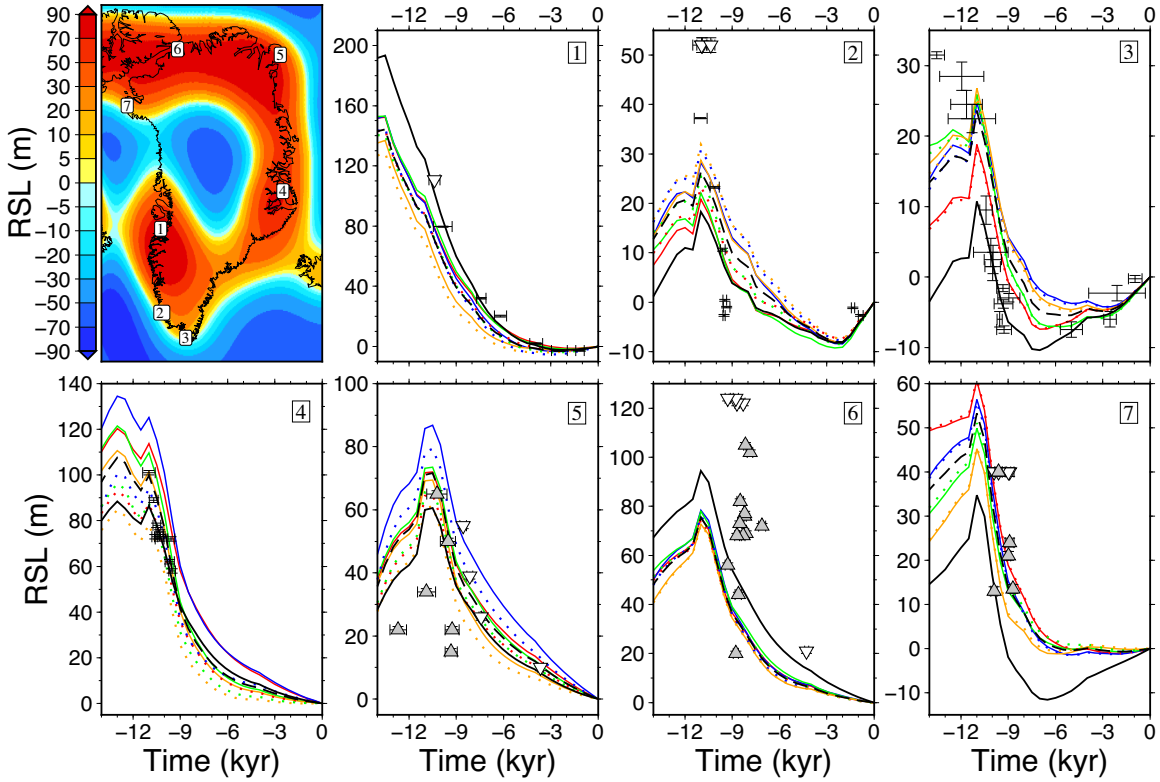

Figure 3. Top-left frame shows RSL at 10 kyr BP based on the reference earth viscosity model. The other frames show model output of RSL at seven locations (shown in top-left frame) around Greenland. These are selected from the analysis of Lecavalier *et al.* (2014) and are numbered to follow the order defined in that analysis: 1 is site 6 (Innaarsuit); 2 is site 13 (Paamiut); 3 is site 16 (Nanortalik); 4 is site 19 (Schuchert); 5 is site 30 (Kronprins); 6 is site 39 (Hall West); 7 is site 43 (Saunders). For each locality, ten curves are indicated: the reference model (solid black line) as well as those corresponding to the eight models with lateral structure (coloured lines) and the mean of these (black dashed line). The lithosphere model adopted in the 3-D earth model runs is indicated via solid colour lines (Zhong *et al.* 2003) and dashed lines (Conrad & Lithgow-Bertelloni 2006). The colour coding is as follows: S40RTS (red lines), Savani (blue lines), SEMUCB-WM1 (green lines), SL2013sv (orange lines). Three types of RSL observations are also indicated: index points that accurately define the time and height of ancient sea level are shown as crosses (with time and height error bars) and limiting data are indicated by darker grey triangles (lower limiting) and lighter grey inverted triangles (upper limiting). The limiting data indicate the height that sea level was above (lower limiting) or below (upper limiting) at a given time and represent a less precise measure of RSL compared to the index points. See Section 2.2 of Lecavalier *et al.* (2014) for further information on the RSL observations.

(i.e. nn9894 as opposed to nn9927 from Tarasov *et al.* (2012)). The seven localities were chosen to provide a good indication of the spatial variability in RSL change around the island. They were also chosen to highlight locations where the Huy3 ice history and partnering 1-D earth model does not produce good quality fits to the data—specifically, in the south (sites 2 and 3) and north (sites 5, 6 and 7) of Greenland. The results in Fig.3 show that the amplitude of RSL change varies around the Island (peaking at ∼200 m) near Disko Bugt (site 1) and that most areas experienced peak sea levels in the early Holocene followed by a rapid fall that continued to present at some locations or was followed by a rise starting between the mid to late Holocene. The causes of this spatial and temporal variability have been discussed previously (Tarasov & Peltier 2002; Fleming & Lambeck 2004; Simpson *et al.* 2009; Lecavalier *et al.* 2014) and so will not be described here, suffice to say that it reflects the timing and geometry of past changes in Greenland and other ice sheets. The primary importance of the 1-D model results here is that they serve to define a reference to gauge the importance of adding lateral viscosity structure to the earth model. We will return to Fig. 3 towards the end of this section to discuss the contributions of lateral structure to the model output at each locality.

We begin by examining the influence of lateral structure over two different depth ranges in the sublithospheric mantle. Fig. 4 shows model output of RSL at 10 kyr BP relative to the 1-D reference model for viscosity structure calculated using S40RTS and a uniform lithosphere of thickness 120 km. The influence of lateral viscosity structure between 120 and ∼2800 km (Fig. 4a) is characterized by RSL values that are lower by up to ∼20 m in most parts of the coast but also higher in some areas, notably southeast Greenland and the mid-west to northwest. Relating this signal to the lateral viscosity structure in this model is difficult given that the pattern and sign of the viscosity perturbations change with depth (as crudely illustrated in the three depth 'slices' included in Fig. S1 of the Supporting Information). Separating the signal into that associated with structure in the lower (Fig. 4b) and upper mantle (Fig. 4c) makes it possible to delineate the relative contribution of structure in these regions to the net signal (Wu 2005; Wang & Wu 2006). As one would expect, the component signal from lower-mantle structure is of longer wavelength compared to that for the upper mantle. The greater amplitude of the upper-mantle contribution reflects the spatial scale of the load changes within the Greenland ice sheet during the most recent deglaciation, rather than changes in the amplitude of lateral viscosity structure with depth. Although not demonstrated here, the substantial sensitivity to lower-mantle structure is probably dominated by deformation associated with the adjacent North American ice sheets (Fleming & Lambeck 2004; Simpson *et al.*

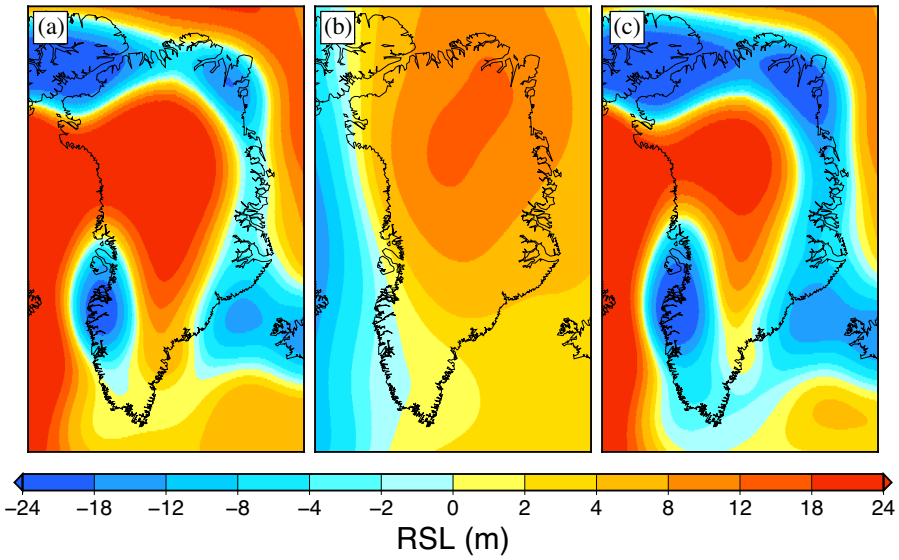

Figure 4. Model output of RSL at 10 kyr BP relative to the 1-D reference model for lateral viscosity structure based on the S40RTS velocity model and a uniform lithosphere of thickness 120 km. The sublithosphere lateral viscosity structure is distributed over different depth extents: (a) base of lithosphere to ∼2800 km depth, (b) 670 to ∼2800 km and (c) base of lithosphere to 670 km.

2009; Lecavalier *et al.* 2014). In the majority of coastal regions, the influence of structure in the upper and lower mantle has the opposite sign thus diminishing the net signal. The signals add along the northern part of the west coast to produce RSL values that are over 20 m higher than those produced by the 1-D model.

Adding a lithosphere with lateral structure to the S40RTS viscosity model produces significant changes to the predicted RSL values at 10 kyr BP (Fig. 5). The greatest differences between the two lithosphere thickness models considered here (Zhong *et al.* 2003; Conrad & Lithgow-Bertollini 2006) are found to the east of Greenland as the lithosphere thins towards the mid-Atlantic ridge (Fig. 1). This is reflected in Fig. 5, which shows that the greatest differences (between all three cases) are in eastern Greenland (and Iceland). In most parts of the east Greenland coast, adding lateral structure to the lithosphere acts to reduce the negative RSL values associated with sublithosphere structure. This effect is more pronounced with the Zhong *et al.* model, for which positive RSL values (relative to the 1-D reference model) are produced for a large swath of the east Greenland coast. The influence of lateral structure elsewhere is more subtle due to the dominant signal associated with lateral viscosity structure in the upper mantle and the smaller differences between the uniform and lateral lithosphere models over much of central and western Greenland.

The results in Figs 4 and 5 indicate that lateral viscosity structure in both the lithosphere and sublithospheric mantle have a significant effect on model output of RSL and that upper-mantle structure has the dominant influence in most regions. Due to computational resource constraints, we did not compute similar depth sensitivity results for the other seismic models. While we expect there to be some differences, the general conclusion that upper-mantle structure is dominant will likely be the same for all models. The influence of lateral structure for all four seismic models considered is shown in Figs S5 and S6 (Supporting Information). Comparison of the results shown in these figures illustrates that, although there are some similarities in the predicted structure, there are also some considerable differences. To better isolate both the similarities and differences of these results, we computed the mean and standard deviation using all eight realizations of lateral structure; the former can be considered as our best estimate of the influence of lateral structure while the latter is a measure of the uncertainty in this estimate. We show the mean RSL minus the reference 1-D result and well as twice the calculated standard deviation in Fig. 6. The mean of the eight 3-D model runs brings out the aspects of the signal that are relatively robust, such as the two regions of lower than average RSL in central west and northwest Greenland, as well as the region of greater than average RSL values in between these west coast sectors. In terms of signal uncertainty, the greatest values are produced for the east coast between the RSL sites 4 and 5 and on the west coast between sites numbered 1 and 7. We note that the amplitude of the estimated uncertainty is greater than the mean value in some areas, such as along the central and northern east coast and the central west coast.

Fig. 3 provides temporal context for the spatial patterns shown in Fig. 6. At six of the seven locations considered, the influence of lateral structure—as defined by the mean of all eight model runs (dashed black line) relative to the height of the reference (1-D) model (solid black line)—does not change sign over the period shown; site 4 is the exception. When considering individual runs (coloured lines), it remains true that in the majority of cases the sign of the influence of lateral structure is constant through time but there are more examples where the sign does change. At most sites, the individual model runs indicate a consistent bias of higher or lower RSL values regardless of the lateral structure imposed. The time-series of individual model runs provides useful information on the cause of the spread in the output (as shown in Fig. 6b at 10 kyr BP). At some locations (e.g. 4), the vertical spread is dominated by the two lithosphere thickness models used, whereas at others (e.g. 3, 7), the contribution from lateral variations beneath the lithosphere is more important. At some sites, the mean influence of lateral structure (dashed black line) is larger than the model spread associated with the input seismic and lithosphere models (1, 3, 6 and 7) but not others (2, 4 and 5).

The results in Figs 3 and 6 can be used to determine whether lateral structure can account for the primary data model misfits identified in Lecavalier *et al.* (2014); specifically, the low modelled RSL values during the early Holocene in southern (sites 2 and 3) and

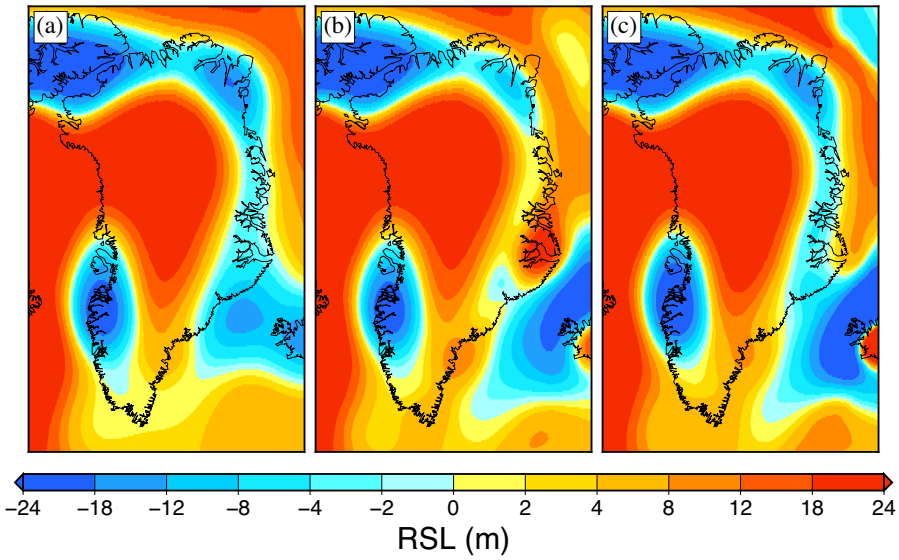

Figure 5. Model output of RSL at 10 kyr BP relative to the 1-D reference model for the 3-D model with lateral structure based on the S40RTS seismic model. The results in each frame indicate a different elastic lithosphere used in each case: (a) uniform with thickness 120 km, (b) non-uniform based on the Zhong *et al.* (2003) model and (c) non-uniform based on the Conrad & Lithgow-Bertollini (2006) model.

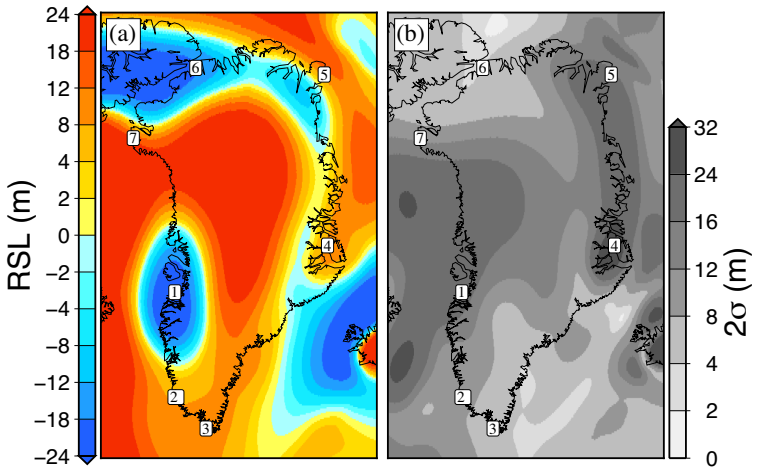

Figure 6. (a) The mean of 3-D model output based on eight realizations of lateral viscosity structure relative to the reference 1-D model. (b) Twice the standard deviation of the model output based on the eight runs of 3-D viscosity structure. The numbers (1–7) indicate the locations of the model RSL curves and observations shown in Fig. 3.

northern (sites 5, 6 and 7) Greenland. In southern Greenland, the influence of lateral structure raises the modelled RSL during the early Holocene for all of the lateral structures considered, thus reducing the data model discrepancy in terms of matching the amplitude of the local RSL signal. However, even the models that maximize RSL in the early Holocene still fall considerably short of the observed values and the general shape of modelled RSL curves does not match well the shape suggested by the observations. At Paamiut (site 2), the observed rate of RSL fall is not well matched by any of the models suggesting that the misfit is dominated by limitations in the ice model (Lecavalier *et al.* 2014; Woodroffe *et al.* 2014). At Nanortalik (site 3), a key issue appears to be the timing of initial ice model deglaciation: a better fit would be possible by deglaciating about 3 kyr earlier. Thus, our results suggest that the lateral viscosity structure considered here cannot resolve the misfits associated with a 1-D earth model in southern Greenland, implying that the ice history is inaccurate (Woodroffe *et al.* 2014) and/or other processes not included in the model are active (e.g. Steffen *et al.* 2014).

At the northern sites (5, 6 and 7), the data quality is relatively poor with an absence of index points. However, the upper- and lower-limiting data are sufficient to indicate that the reference model curves are incompatible with the observations in terms of both the amplitude and timing of RSL fall. Adding lateral structure increases the amplitude of the RSL fall at sites 5 and 7 and so can reconcile this aspect of the data model misfit. At site 6, however, the amplitude is decreased and so the residuals are increased by adding lateral structure. At site 5, some of the individual model runs provide good fits to the limiting data. At site 7, our results suggest that delaying the deglaciation by ∼1 kyr would produce improved fits. Our results for site 6 suggest that the ice history is the likely source of the poor fits at this locality; specifically, greater and delayed ice thinning would result in more accurate model curves. Greater ice thinning in the area is supported by loss of ice buttressing with the

Innuitian ice sheet when Nares Strait deglaciated (MacGregor *et al.* 2016) and the elevated early Holocene temperatures compared to those estimated at the GRIP ice core site (Lecavalier *et al.* 2017). Of course, revising the ice history in this way will also impact the predicted RSL curve at site 7 and so fitting the RSL data at all sites in northwest Greenland will be a challenge.

Thus far, we have considered locations where the reference model did not provide good fits to the RSL observations to assess whether adding lateral structure can resolve the misfits. It is also instructive to examine the change to model output where the reference model produced relatively good fits to the RSL data to consider the implications regarding potential biases in the ice model. The greatest density of high-quality RSL data is found in and surrounding Disko Bugt (site 1 and vicinity). At this location, lateral structure reduces the modelled amplitude of RSL fall for all model runs. The simplest interpretation of this result is that, by not considering lateral Earth structure, the inference of ice thickness in this region is biased low and/or timing of deglaciation is biased early. While these are certainly possibilities, ice modelling sensitivity tests would be required to determine whether such changes to the ice model are compatible with other constraints, such as those on the location and timing of margin retreat in this area (Lecavalier *et al.* 2014). At site 4, the addition of lateral structure results in an improved fit to the RSL data by increasing the amplitude and thus capturing the oldest RSL index points comfortably. The average of the 3-D model runs produces a high quality fit to these data.

In developing the Huy2 model, Simpson *et al.* (2009) found that it was difficult to produce good fits to RSL observations on both the east and west coasts with the Huy2 ice model reconstruction. They proposed that this reflected either a difference in viscosity structure between the two coasts or asynchronous retreat of the ice margin, with earlier retreat in the east. Lecavalier *et al.* (2014) tested this second hypothesis by implementing spatial variation in the sensitivity of the ice model to the applied sea level forcing and found that good fits could be achieved to data on both coasts by producing an earlier retreat in the east. Our results indicate that lateral Earth structure is not a viable explanation for the east–west issue noted by Simpson *et al.* (2009) in that it leads to, on average during the early Holocene, a shift of the modelled RSL curves to older times in the Disko Bugt area where the majority of RSL data are located (site 1) and earlier times in the east (e.g. sites 4 and 5). That is, adding lateral structure would replicate an earlier margin retreat in the Disko Bugt area compared to the east coast, the opposite of the change required to better fit the observations. Thus, our results provide further support for an earlier retreat of the ice margin in the east compared to the west (Disko Bugt region) and are compatible with ice margin chronology constraints (Funder *et al.* 2011; Sinclair *et al.* 2016) and evidence for earlier ocean warming along the east coast (Williams 1993; Knutz *et al.* 2011).

3.2 Present-day vertical land motion and gravity changes

In considering the influence of lateral Earth structure on model output of present-day rates of vertical land motion, we follow a very similar progression to that in the previous section. Thus, we begin by first considering results for the S40RTS model and a uniform, 120 km thick elastic lithosphere. The influence of this realization of lateral structure (relative to the 1-D reference case) can reach values with amplitude in excess of 1 mm yr^{-1}, with subsidence in the northwest and southeast and uplift in the central west of Greenland. As for RSL (Fig. 4), lateral structure in the upper mantle (Fig. 7c) dominates the total signal (Fig. 7a). The component signal associated with lateral structure in the lower mantle (Fig. 7b) contributes no more than a few tenths of a mm yr^{-1}. As for the case of RSL, adding lateral structure to the lithosphere does not dramatically influence the general pattern associated with sublithosphere structure but it can make a significant contribution in areas where there are large differences between the uniform and non-uniform models. For example, application of the Zhong *et al.* (2003) model (Fig. 8b) increases the rate of uplift in central to northern parts of the east coast by up to 1.5 mm yr^{-1}.

Comparing the influence of lateral structure for all four seismic models (Figs S7 and S8, Supporting Information) on present-day vertical land motion indicates that some features in the signal are robust across all models, such as subsidence in northwest Greenland and uplift south of this area, but there are also some significant differences. Rates based on the Savani model are an outlier in that this is the only model that predicts uplift along the entire east coast regardless of the adopted lithosphere thickness model. The differences between the model output shown in Figs S7 and S8 of the Supporting Information indicate relatively large uncertainty in quantifying the influence of lateral structure on present-day vertical land motion. This is apparent in Fig. 9 which shows the mean (Fig. 9b) and (twice the) standard deviation (Fig. 9c) of the model output for all eight realizations of lateral structure considered here.

The results in Fig. 9 indicate that the influence of lateral structure, as defined by the mean of the eight models relative to the 1-D reference case (Fig. 9b), is a fraction of the total signal obtained from the reference model (Fig. 9a) in most locations where GPS receivers have been deployed (Bevis *et al.* 2012). However, there are some locations where the component signal due to lateral structure (Fig. 8b) is similar in magnitude to the total signal (e.g. central western Greenland). The averaging process brings out the more robust features of the signal due to lateral Earth structure. In particular, the amplitudes of subsidence in the northwest and uplift south of this region are greater than the estimated uncertainty (Fig. 9c). For the majority of the Greenland coast where GPS stations are located, the average influence of the lateral structure considered here results in land uplift of less than 1 mm yr^{-1}. The 2-sigma uncertainty estimate is generally at the sub-mm yr^{-1} level for most of the Greenland coast, except in central to northern parts of the east where there are values exceeding 2 mm yr^{-1}. The spread in model output as represented by twice the standard deviation is of similar amplitude to, and often larger than, the mean influence of lateral structure on present-day vertical land motion.

A recent study estimated land uplift rates due to GIA (Khan *et al.* 2016) by estimating and subtracting the signal associated with elastic motion due to ice thickness changes during the monitoring period. One result of the Khan *et al.* (2016) study is that uplift rates predicted by GIA models that were tuned to fit RSL and ice extent data do not produce good fits to the calculated rates at the majority of sites. This discrepancy is evident in Fig. 10 which compares the GIA rates from Khan *et al.* (2016; their Table S1) to those from our reference model (essentially the Huy3 model of Lecavalier *et al.* 2014). The data and model results are plotted at sites in sequence with the drainage basins (1–7) identified in Khan *et al.* (2016). For clarity, the data model comparison is split into two frames. Inspection of Fig. 10 shows that the reference model does not fit the GPS-inferred GIA rates at any of the 54 sites. The discrepancy (GPS-inferred minus modelled) ranges from about 10 mm yr^{-1} to around 1 mm yr^{-1}. The two sites (25 and 26) where the discrepancy is largest are somewhat anomalous in the sense that the GPS-inferred rates are significantly higher than at other sites. It

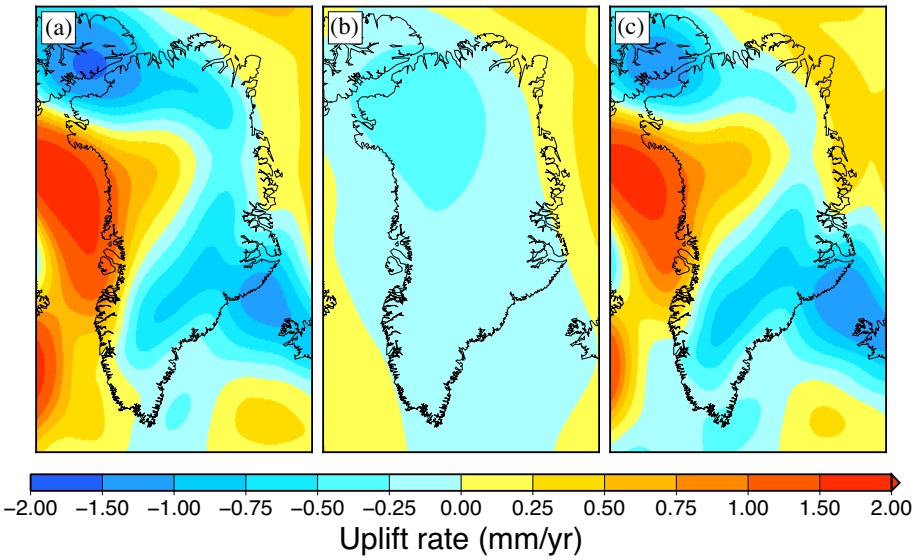

Figure 7. Model output of present-day uplift rate relative to the 1-D reference model for lateral viscosity structure based on the S40RTS velocity model and a uniform lithosphere of thickness 120 km. The sublithosphere lateral viscosity structure is distributed over different depth extents: (a) base of lithosphere to ∼2800 km depth, (b) 670 km to ∼2800 km and (c) base of lithosphere to 670 km.

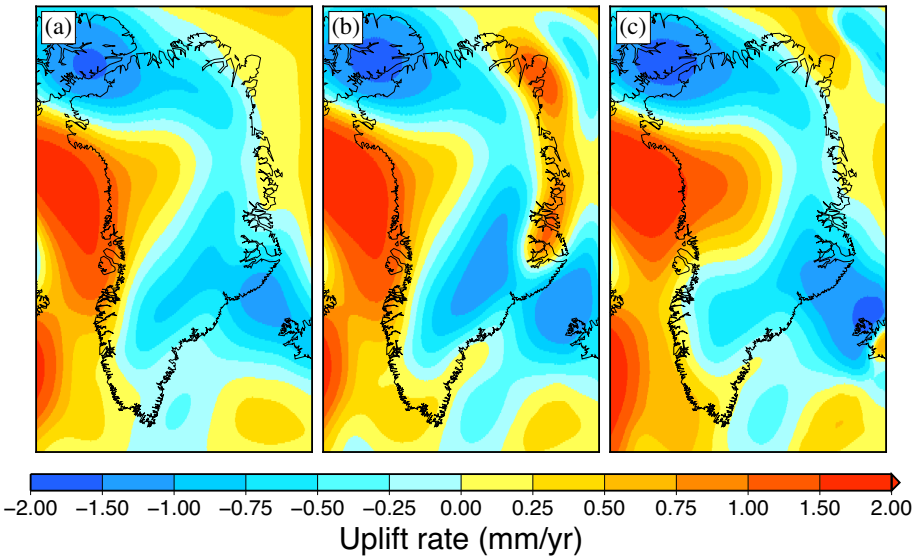

Figure 8. Model output of present-day uplift rate relative to the 1-D reference model for the 3-D model with lateral structure based on the S40RTS seismic model. The results in each frame indicate a different elastic lithosphere used in each case: (a) uniform with thickness 120 km, (b) non-uniform based on the Zhong *et al.* (2003) model and (c) non-uniform based on the Conrad & Lithgow-Bertollini (2006) model.

has been suggested that this is due to a large signal associated with local ice thinning in the 20th century combined with low viscosity values in regions where Greenland passed over the plume presently located under Iceland (Khan *et al.* 2016 and references therein). The models used to infer lateral structure here do not have the required resolution to infer lateral variations on these scales.

Adding lateral structure to the reference earth model does not make a significant improvement to the overall data model fit (Fig. 10). At the majority of sites, where the discrepancy is greater than ∼2 mm yr^{-1}, the amplitude of change associated with adding lateral structure is too small to explain the residuals. In some locations where the residuals are less large (e.g. sites 8–17), some of the 3-D models fall within the data uncertainty range. In terms of our 'best estimate' model (mean of all eight 3-D models), none fit the GPS-inferred rates; at some locations the fit is improved (e.g. sites 48–54), while at others it is made worse (e.g. sites 1–5). As noted in Section 2.1, the model reference frame used to compute vertical land motion is different to that used in arriving at the GPS-inferred rates. This could lead to an approximately uniform offset between the modelled and GPS-inferred rates but with amplitude at the sub-mm yr^{-1} level, which is considerably less than the residuals shown in Fig. 10. Some of the discrepancies indicated in Fig. 10 reflect the fact that our reference GIA model (Lecavalier *et al.* 2014) was constructed to match paleo ice extent and RSL reconstructions and not GPS-inferred uplift rates. Indeed, some of the areas with large residuals correspond to those where there are no RSL data (mid-to-north section of the west coast; sites 46–54) or where the model fits are relatively poor (western part of north coast; sites 1–4). A

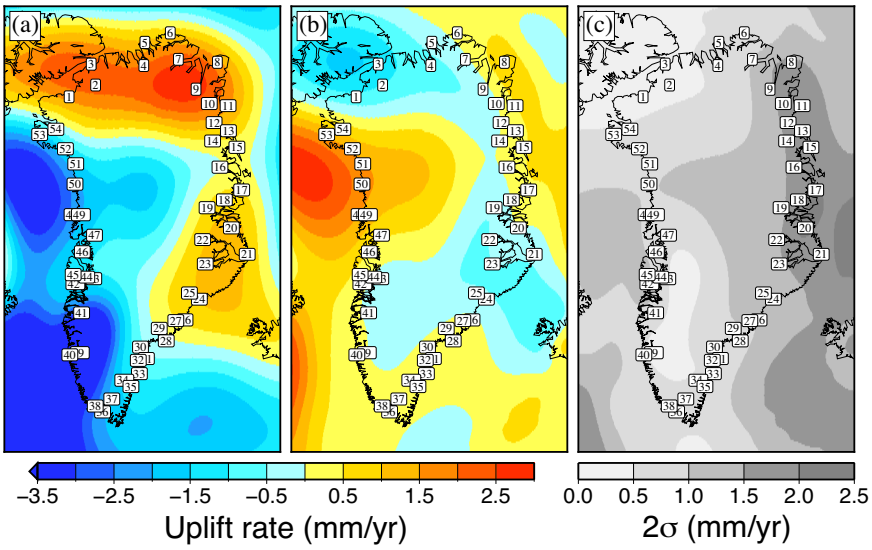

Figure 9. (a) Present-day uplift rates generated by the reference 1-D earth model. (b) The mean of 3-D model output based on eight realizations of lateral viscosity structure relative to the reference 1-D model. (c) Twice the standard deviation of the model output based on the eight runs with 3-D viscosity structure. The numbers (1–54) indicate the locations of GNET GPS stations (Bevis *et al.* 2012). These are numbered in sequence with the drainage basins defined in Khan *et al.* (2016). Comparison of the model uplift rates to those inferred from the GNET GPS stations is provided in Fig. 10.

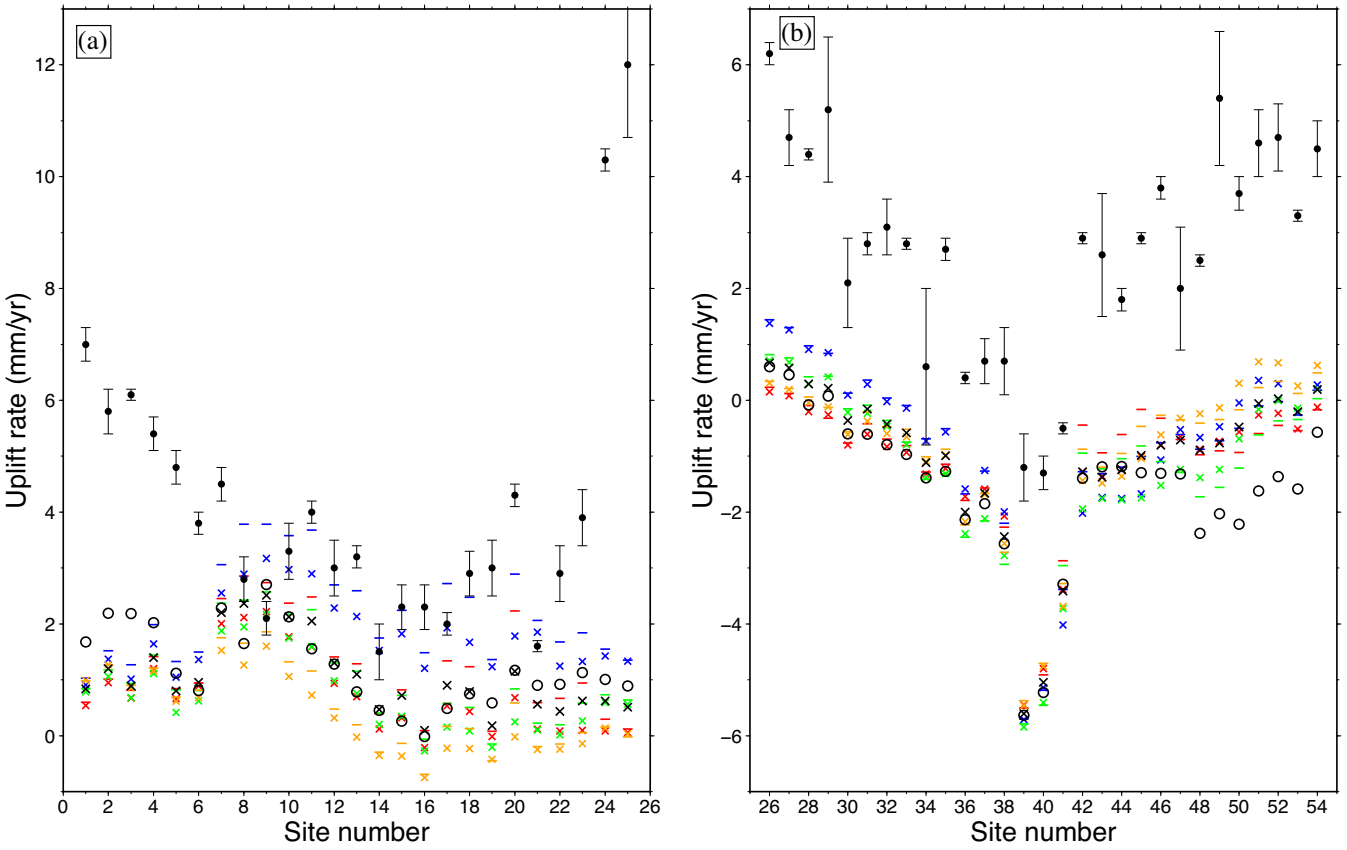

Figure 10. Comparison of GPS-inferred and modelled uplift rates at the sites of the GNET stations (see Fig. 9 for locations). The rates inferred from the GPS time-series (corrected for elastic motion during the monitoring period) are shown as solid circles with their associated uncertainty (Khan *et al.* 2016). Results for the 1-D reference model are indicated by black circles and the 3-D model output is given by coloured symbols. The mean of the eight 3-D model runs is indicated by the black 'x' symbol for each site. The lithosphere model adopted in the 3-D earth model runs is indicated via coloured dashes (Zhong *et al.* 2003) and coloured 'x' symbols (Conrad & Lithgow-Bertelloni 2006). The colour coding is as follows: S40RTS (red), Savani (blue), SEMUCB-WM1 (green) and SL2013sv (orange). For clarity, figure is split into two frames: (a) sites 1–25 and (b) sites 26–54.

recent study has shown that the Huy3 model likely underestimates ice thinning in this area due to an underestimate in the temperature forcing (Lecavalier *et al.* 2017) and that a revised model accounting for this increases the predicted uplift rates by about 2 mm yr^{-1}. However, this does not resolve the data model discrepancy as the influence of lateral structure is to decrease modelled rates in this region. There are also locations where the reference model fits the RSL data well and yet there remain large differences in the modelled and GPS-inferred uplift rates. Central western Greenland is a good example. One interpretation of the RSL results in Fig. 3 is that the ice model underestimates the amount of mass loss in this region. This suggests one avenue to improve the model fits to the GPS data; however, a key constraint is the observed minimum in RSL and rise to present during the past few kyr. This can only be achieved by a regrowth of the ice sheet large enough to overprint the uplift associated with the earlier retreat. Thus, in this region at least, the only alternative to simultaneously fitting the RSL and GPS observations is to consider relatively recent (past century or so) changes in the ice sheet (Kjeldsen *et al.*, 2015). Resolving the discrepancies shown in Fig. 10 is an important challenge for future study.

To end this section, we briefly consider the impact of lateral structure on estimating present-day ice mass loss in different sectors of the Greenland ice sheet via Gravity Recovery and Climate Experiment (GRACE) observations. Estimates of the GIA contribution to mass changes for 19 sectors of the ice sheet are shown in Fig. 11. The interior boundaries are based on the Greenland Ice Sheet Drainage Basins of Zwally *et al.* (2012) and the external regions cover the remaining areas to the coasts. The rate of change of mass for each region is calculated using a similar method to that used by Jacob *et al.* (2012) for assessing geoid change. This method is commonly employed to assess mass changes using data from the GRACE mission. Unlike a typical GRACE data analysis that must deal with issues associated with data noise and uncertainty via processing techniques (e.g. smoothing, filtering), our analysis here does not require the use of these techniques since we are dealing directly with model output (at the relatively high spherical harmonic truncation of degree and order 512).

The GIA signal (as computed for the 1-D reference model) is on the order of a few Gt yr^{-1} which is generally within the uncertainty of the mass loss values estimated for the drainage basins (e.g. Xu *et al.* 2016). In the majority of the areas defined in Fig. 11, the average influence of lateral structure is to increase the GIA signal. The largest shift in the mean (position of black crosses relative to the black circles in Fig. 11) is ∼1 Gt yr^{-1} for area number 5, as a result of this mascon correlating strongly with the region of uplift associated with lateral structure (Fig. 9b). When considering individual model runs, differences from the 1-D reference case reaches ∼1.5 Gt yr^{-1} for some areas (5 and 13). Thus, the lateral structure considered here can produce changes in the GIA contribution to mass changes that are of similar magnitude to the total (GIA) signal. However, since the GIA contribution is a relatively small effect overall (assuming our reference 1-D model is accurate), the impact on estimates of recent mass changes in the ice sheet will be within uncertainty in most drainage basins.

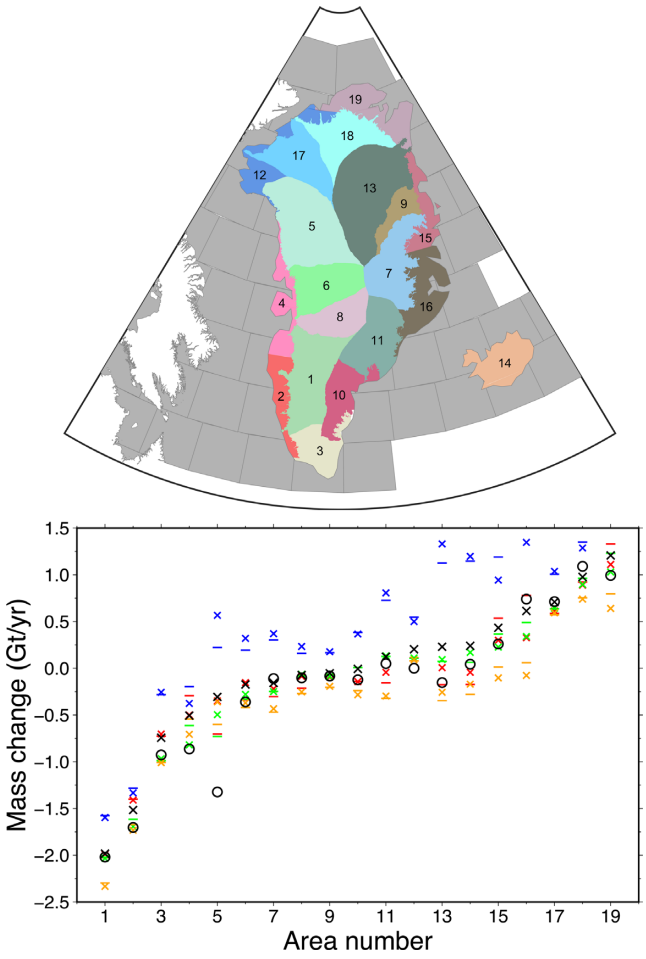

Figure 11. Map shows the 19 drainage basin areas considered in the bottom frame (the *x*-axis). Plot shows rates of mass change inferred from model output. Results for the 1-D reference model are indicated by black circles and the 3-D model output is given by coloured symbols. The mean of the eight 3-D model runs is indicated by the black 'x' symbol for each area. The lithosphere model adopted in the 3-D earth model runs is indicated via coloured dashes (Zhong *et al.* 2003) and coloured 'x' symbols (Conrad & Lithgow-Bertelloni 2006). The colour coding is as follows: S40RTS (red), Savani (blue), SEMUCB-WM1 (green) and SL2013sv (orange).

4 CONCLUDING REMARKS

We present the first results that consider the influence of lateral Earth structure on Greenland GIA using a model that can explicitly incorporate this structure. In total, eight realizations of lateral viscosity structure were developed using four global seismic velocity models and two global lithosphere (elastic) thickness models. The influence of lateral structure was determined by comparing model output from these eight models to that of a model with no lateral structure but with the same (global scale) depth-dependent viscosity structure as the 3-D models.

Our results show that lateral viscosity structure both in the lithosphere (in terms of the elastic thickness) and in the sublithospheric mantle have a significant influence on model output of both deglacial RSL changes and present-day vertical land motion. For example, lateral structure affects RSL predictions in the early Holocene by several tens of metres in many locations resulting in enhanced RSL values relative to the 1-D case. In two areas (northwest Greenland and the Disko Bugt region), lateral structure results in a decrease in RSL values. Model output of present-day vertical land motion show departures from the 1-D case at the mm yr^{-1} level in many locations and exceeds values of 2 mm yr^{-1} in some areas such as the northwest coast.

The signals associated with lateral viscosity structure have implications for interpreting the observed changes in RSL and uplift rate. For example, our results support the interpretation for an asynchronous retreat of the Greenland ice sheet during the most recent deglaciation, with retreat of the eastern margin occurring several kyr earlier than that in the west. Furthermore, our results suggest that lateral Earth structure is unable to account for the discrepancies in northwest and southern Greenland highlighted by Lecavalier *et al.* (2014), indicating limitations in the Huy3 ice model reconstruction and/or the importance of processes not included in our model (e.g. GIA-induced faulting; Steffen *et al.* 2014). Regarding present-day uplift rates, our results show that large discrepancies exist between those output from our reference 1-D model and those inferred from GPS data; these discrepancies cannot be reconciled by adding the realizations of lateral structure considered here. Further work is required to determine if a single GIA model can fit both the GPS and RSL data constraints.

The spread in model output for the eight different realizations of lateral structure is of similar amplitude to the influence of lateral structure (as defined by the average of all eight model runs) in many areas. This reflects the differences between the four seismic and two lithosphere models used and leads to a relatively large uncertainty associated with these aspects in defining the GIA signal. Other aspects not considered here, such as uncertainty in the scaling between seismic velocity and viscosity, will also contribute to the uncertainty in defining lateral variations and hence model output. The uncertainty in defining lateral structure will likely be reduced when higher resolution models of lithosphere thickness and mantle velocity structure are made available for the Greenland region. Indeed, a clear next step is to develop more accurate constraints on Earth structure based on regional geophysical data sets.

ACKNOWLEDGEMENTS

GAM acknowledges funding support from the Natural Sciences and Engineering Research Council of Canada, the Canada Research Chairs Program and the University of Ottawa. This paper is a contribution to the PAGES/INQUA funded PALSEA2 working group and the SCAR SERCE program.

REFERENCES

Argus, D.F, 2012. Uncertainty in the velocity between the mass center and surface of Earth, *J. Geophys. Res. Solid Earth* **117,** doi:10.1029/2012JB009196.

Auer, L., Boschi, L., Becker, T.W., Nissen-Meyer, T. & Giardini, D., 2014. *Savani*: A variable resolution whole-mantle model of anisotropic shear velocity variations based on multiple data sets, *J. geophys. Res.,* **119,** 3006–3034.

Bevis, M. *et al.*, 2012. Bedrock displacements in Greenland manifest ice mass variations, climate cycles and climate change, *Proc. Natl. Acad. Sci. USA,* **109,** 11 944–11 948.

Blewitt, G., 2003. Self-consistency in reference frames, geocenter definition, and surface loading of the solid Earth, *J. Geophys. Res. Solid Earth* **108**(B2), doi:10.1029/2002JB002082.

Cammarano, F., Tackley, P. & Boschi, L., 2011. Seismic, petrological and geodynamical constraints on thermal and compositional structure of the upper mantle: global thermochemical models, *Geophys. J. Int.,* **187,** 1301–1318.

Chopelas, A. & Boehler, R., 1992. Thermal expansivity in the lower mantle, *Geophys. Res. Lett,* **19,** 1983–1986.

Conrad, C.P. & Lithgow-Bertelloni, C., 2006. Influence of continental roots and asthenosphere on plate-mantle coupling, *Geophys. Res. Lett.,* **33,** L05312, doi:10.1029/2005GL025621.

Dziewonski, A.M. & Anderson, D.L., 1981. Preliminary reference Earth model, *Phys. Earth planet. Inter.,* **25**(4), 297–356.

Fleming, K. & Lambeck, K., 2004. Constraints on the Greenland ice sheet since the Last Glacial Maximum from sea-level observations and glacial-rebound models, *Quat. Sci. Rev.,* **23**(9–10), 1053–1077.

Forte, A.M. & Woodward, R.L., 1997. Seismic-geodynamic constraints on three-dimensonal structure, vertical flow, and heat transfer in the mantle, *J. geophys. Res.,* **102,** 17 981–17 994.

French, S. & Romanowicz, B., 2014. Whole-mantle radially anisotropic shear-velocity structure from spectral-element waveform tomography, *Geophys. J. Int.,* **199,** 1303–1327.

Funder, S., Kjeldsen, K.K., Kjær, K.H. & O'Cofaigh, C., 2011. The Greenland ice sheet during the past 300,000 years: a review, in *Quaternary Glaciations - Extent and Chronology: A Closer Look,* Vol. **15,** pp. 699–713, eds Ehlers, J., Gibbard, P.L. & Hughes, P.D., Elsevier.

Ivins, E.R. & James, T.S., 2005. Antarctic glacial isostatic adjustment: a new assessment, *Antarct. Sci.,* **17,** 541–553.

Ivins, E.R. & Sammis, C.G., 1995. On lateral viscosity contrast in the mantle and the rheology of low frequency geodynamics, *Geophys. J. Int.,* **123,** 305–322.

Jacob, T, Wahr, J., Gross, R., Swenson, S. & A, G., 2012. Estimating geoid height change in North America: past, present and future, *J. Geod.,* **86,** 337–358.

Karato, S., 1993. Importance of anelasticity in the interpretation of seismic tomography, *Geophys. Res. Lett.,* **20,** 1623–1626.

Karato, S., 2008. *Deformation of Earth Materials: An Introduction to the Rheology of the Solid Earth,* pp. 463, Cambridge Univ. Press.

Kaufmann, G., Wu, P. & Ivins, E.R., 2005. Lateral viscosity variations beneath Antarctica and their implications on regional rebound motions and seismotectonics, *J. Geodyn.,* **39**(2), 165–181.

Kendall, R.A., Mitrovica, J.X. & Milne, G.A., 2005. On post-glacial sea level–II. Numerical formulation and comparative results on spherically symmetric models, *Geophys. J. Int.,* **161**(3), 679–706.

Kennett, B.L.N., Engdahl, E.R. & Buland, R., 1995. Constraints on seismic velocities in the Earth from travel times, *Geophys. J. Int.,* **122,** 108–124.

Khan, S.A. *et al.*, 2016. Geodetic measurements reveal similarities between post-Last Glacial Maximum and present-day mass loss from the Greenland ice sheet. *Sci. Adv.,* **2**(9), e1600931, doi:10.1126/sciadv.1600931.

Kjeldsen, K.K. *et al.*, 2015. Spatial and temporal distribution of mass loss from the Greenland ice sheet since AD 1900, *Nature,* **528,** 396–400.

Knutz, P.C., Sicre, M.A., Ebbesen, H., Christiansen, S. & Kuijpers, A., 2011. Multiple-stage deglacial retreat of the southern Greenland ice sheet linked with Irminger current warm water transport, *Paleoceanography,* **26,** PA3204, doi:10.1029/2010PA002053.

Lambeck, K., Smither, C. & Johnston, P., 1998. Sea-level change, glacial rebound and mantle viscosity for northern Europe, *Geophys. J. Int.,* **143,** 102–144.

Latychev, K., Mitrovica, J.X., Tromp, J., Tamisiea, M.E., Komatitsch, D. & Christara, C.C., 2005. Glacial isostatic adjustment on 3-D Earth models: a finite volume formulation, *Geophys. J. Int.,* **161,** 421–444.

Lecavalier, B. *et al.*, 2017. High Arctic Holocene temperature record from the Agassiz ice cap and Greenland ice sheet evolution, *Proc. Natl. Acad. Sci. USA,* **114,** 5952–5957.

Lecavalier, B.S. *et al.*, 2014. A model of Greenland ice sheet deglaciation constrained by observations of relative sea level and ice extent, *Quat. Sci. Rev.,* **102,** 54–84.

Long, A.J., Woodroffe, S.A., Roberts, D.H. & Dawson, S., 2011. Isolation basins, sea-level changes and the Holocene history of the Greenland ice sheet, *Quat. Sci. Rev.,* **30**(27–28), 3748–3768.

MacGregor, J.A., Colgan, W.T., Fahnestock, M.A., Morlighem, M., Catania, G.A., Paden, J.D. & Gogineni, S.P., 2016. Holocene deceleration of the Greenland Ice Sheet, *Science,* **351**(6273), 590–593.

Milne, G.A., Davis, J.L., Mitrovica, J.X., Scherneck, H.-G., Johansson, J.M., Vermeer, M. & Koivula, H., 2001. Space-geodetic constraints on glacial isostatic adjustment in Fennoscandia, *Science,* **291,** 2381–2385.

Milne, G.A. & Mitrovica, J.X., 1998. Postglacial sea-level change on a rotating Earth, *Geophys. J. Int.,* **133**(1), 1–19.

Mitrovica, J.X., 1996. Haskell [1935] revisited, *J. geophys. Res.,* **101,** 555–569.
Mitrovica, J.X., Wahr, J., Matsuyama, I. & Paulson, A., 2005. The rotational stability of an ice-age Earth, *Geophys. J. Int.,* **161,** 491–506.
Paulson, A., Zhong, S. & Wahr, J., 2007. Inference of mantle viscosity from GRACE and relative sea level data, *Geophys. J. Int.,* **171,** 497–508.
Peltier, W.R., 2004. Global glacial isostasy and the surface of the ice-age Earth: the ICE-5G (VM2) model and GRACE, *Annu. Rev. Earth planet. Sci.,* **32,** 111–149.
Peltier, W.R. & Andrews, J.T., 1976. Glacial-Isostatic adjustment-I, *Geophys. J. R. astr. Soc.,* **46,** 605–646.
Petrunin, A.G., Rogozhina, I., Vaughan, A.P.M., Kukkonen, I.T., Kaban, M.K., Koulakov, I. & Thomas, M., 2013. Heat flux variations beneath central Greenland's ice due to anomalously thin lithosphere, *Nat. Geosci.,* **6,** 746–750.
Priestley, K. & McKenzie, D., 2013. The relationship between shear wave velocity, temperature, attenuation and viscosity in the shallow part of the mantle, *Earth planet. Sci. Lett.,* **381,** 78–91.
Ritsema, J., Deuss, A., van Heijst, H.J. & Woodhouse, J.H., 2011. S40RTS: a degree-40 shear-velocity model for the mantle from new Rayleigh wave dispersion, teleseismic traveltime and normal-mode splitting function measurements, *Geophys. J. Int.,* **184**(3), 1223–1236.
Schaeffer, A.J. & Lebedev, S., 2013. Global shear speed structure of the upper mantle and transition zone, *Geophys. J. Int.,* **194**(1), 417–449.
Shepherd, A, *et al.*, 2012. A reconciled estimate of ice-sheet mass balance, *Science,* **338**(6111), 1183–1189, doi: 10.1126/science.1228102.
Simpson, M.J.R., Milne, G.A., Huybrechts, P. & Long, A.J., 2009. Calibrating a glaciological model of the Greenland ice sheet from the Last Glacial Maximum to present-day using field observations of relative sea level and ice extent, *Quat. Sci. Rev.,* **28,** 1631–1657.
Sinclair, G., Carlson, A.E., Mix, A.C., Lecavalier, B.S., Milne, G., Mathias, A., Buizert, C. & DeConto, R. 2016. Diachronous retreat of the Greenland ice sheet during the last deglaciation, *Quat. Sci. Rev.,* **145,** 243–258.
Steffen, H., Kaufmann, G. & Wu, P., 2006. Three-dimensional finite-element modelling of the glacial isostatic adjustment in Fennoscandia, *Earth planet. Sci Lett.,* **250,** 358–375.
Steffen, R., Wu, P., Steffen, H. & Eaton, D.W., 2014. The effect of earth rheology and ice-sheet size on fault-slip and magnitude of postglacial earthquakes, *Earth planet. Sci. Lett.,* **388,** 71–80.
Stixrude, L. & Jeanloz, R., 2015. Constraints on seismic models from other disciplines - constraints from mineral physics on seismological models, in *Treatise on Geophysics,* 2nd edn, pp. 829–849, ed. Schubert, G., Elsevier.
Tamisiea, M.E., Mitrovica, J.X. & Davis, J.L., 2007. GRACE gravity data constrain ancient ice geometries and continental dynamics over Laurentia, *Science,* **316,** 881–883.
Tarasov, L., Dyke, A.S., Neal, R.M. & Peltier, W., 2012. A data-calibrated distribution of deglacial chronologies for the North American ice complex from glaciological modeling, *Earth planet. Sci. Lett.,* **315–316,** 30–40.
Tarasov, L. & Peltier, W.R., 2002. Greenland glacial history and local geodynamic consequences, *Geophys. J. Int.,* **150**(1), 198–229.
Tushingham, A.M. & Peltier, W.R., 1991. ICE-3G: a new model of late Pleistocene deglaciation based upon geophysical predictions of post-glacial sea level change, *J. geophys. Res.,* **96,** 4497–4523.
Van der Wal, W., Barnhoorn, A., Stocchi, P., Gradmann, S., Wu, P., Drury, M. & Vermeersen, B., 2013. Glacial isostatic adjustment model with composite 3-D Earth rheology for Fennoscandia, *Geophys. J. Int.,* **194,** 61–77.
Van der Wal, W., Whitehouse, P.L. & Schrama, E.J., 2015. Effect of GIA models with 3D composite mantle viscosity on GRACE mass balance estimates for Antarctica, *Earth planet. Sci. Lett.,* **414,** 134–143.
Wang, H., Wu, P. & van der Wal, W., 2008. Using postglacial sea level, crustal velocities and gravity-rate-of-change to constrain the influence of thermal effects on mantle lateral heterogeneities, *J. Geodyn.,* **46,** 104–117.
Wang, H.S. & Wu, P., 2006. Effects of lateral variations in lithospheric thickness and mantle viscosity on glacially induced relative sea levels and long wavelength gravity field in a spherical, self-gravitating Maxwell Earth, *Earth planet. Sci. Lett.,* **249,** 368–383.
Whitehouse, P., Latychev, K., Milne, G., Mitrovica, J. & Kendall, R., 2006. Impact of 3-D Earth structure on Fennoscandian glacial isostatic adjustment: implications for space-geodetic estimates of present-day crustal deformation, *Geophys. Res. Lett.,* **33,** doi:10.1029/2006GL026568.
Whitehouse, P.L., Bentley, M.J., Milne, G., King, M. & Thomas, I., 2012. A new glacial isostatic adjustment model for Antarctica: calibrated and tested using observations of relative sea-level change and present-day uplift rates, *Geophys. J. Int.,* **190,** 1464–1482.
Williams, K.M., 1993. Ice sheet and ocean interactions, margin of the East Greenland Ice Sheet (14 ka to present): diatom evidence, *Paleoceanography,* **8,** 69–83.
Woodroffe, S.A., Long, A.J., Lecavalier, B.S., Milne, G.A. & Bryant, C.L., 2014. Using relative sea-level data to constrain the deglacial and Holocene history of southern Greenland, *Quat. Sci. Rev.,* **92,** 345–356.
Wu, P., 2005. Effects of lateral variations in lithospheric thickness and mantle viscosity on glacially induced surface motion in Laurentia, *Earth planet. Sci. Lett.,* **235,** 549–563
Wu, P., 2006. Sensitivity of relative sea levels and crustal velocities in Laurentide to radial and lateral viscosity variations in the mantle, *Geophys. J. Int.,* **165,** 401–413.
Wu, P. & Peltier, W.R., 1983. Glacial isostatic adjustmennt and the free air gravity anomaly as a constraint on deep mantle viscosity, *Geophys. J. R. astr. Soc.,* **74,** 377–450.
Wu, P., Wang, H. & Steffen, H., 2013. The role of thermal effect on mantle seismic anomalies under Laurentia and Fennoscandia from observations of Glacial Isostatic Adjustment, *Geophys. J. Int.,* **192**(1), 7–17.
Xu, Z., Schrama, E.J.O., van der Wal, W., van den Broeke, M. & Enderlin, E.M., 2016. Improved GRACE regional mass balance estimates of the Greenland ice sheet cross-validated with the input–output method, *Cryosphere,* **10,** 895–912.
Zhong, S.J., Paulson, A. & Wahr, J., 2003. Three-dimensional finite element modelling of Earth's viscoelastic deformation: effects of lateral variations in lithospheric thickness, *Geophys. J. Int.,* **155,** 679–695.
Zwally, H.J., Giovinetto, M.B., Beckley, M.A. & Saba, J.L., 2012, 'Antarctic and Greenland Drainage Systems, GSFC Cryospheric Sciences Laboratory'. Available at: http://icesat4.gsfc.nasa.gov/cryo_data/ant_grn_drainage_systems.php.

SUPPORTING INFORMATION

Supplementary data are available at *GJI* online.

Figure S1. Lateral variations in viscosity structure calculated using the S40RTS velocity model (Ritsema *et al.* 2011). Viscosity values are relative to those of the reference 1-D model (5×10^{20} Pa s in the upper mantle and 10^{22} Pa s in the lower mantle).

Figure S2. As Fig. S1 except for the Savani velocity model (Auer *et al.* 2014).

Figure S3. As Fig. S1 except for the SEMUCB-WM1 velocity model (French & Romanowicz 2014).

Figure S4. As Fig. S1 except for the SL2013sv velocity model (Schaeffer & Lebedev 2013).

Figure S5. Model output of RSL at 10 kyr BP relative to the 1-D reference model for all of the seismic models considered in this study: (a) S40RTS, (b) Savani, (c) SEMUCB-WM1 and (d) SL2013sv. In each case, the non-uniform lithosphere thickness model of Zhong *et al.* (2003) was used.

Figure S6. As Fig. S5 except for the Conrad & Lithgow-Bertelloni (2006) lithosphere thickness model.

Figure S7. Model output of present-day uplift rate relative to the 1-D reference model for all of the seismic models considered in this study: (a) S40RTS, (b) Savani, (c) SEMUCB-WM1 and (d) SL2013sv. In each case, the non-uniform lithosphere thickness model of Zhong *et al.* (2003) was used.

Figure S8. As Fig. S7 except for the Conrad & Lithgow-Bertollini (2006) lithosphere thickness model.

Please note: Oxford University Press is not responsible for the content or functionality of any supporting materials supplied by the authors. Any queries (other than missing material) should be directed to the corresponding author for the paper.